NMR investigations of Li^+ ion dynamics in the NASICON ionic conductors $Li_{1-x}La_{x/3}\square_{2x/3}Zr_2(PO_4)_3$

2009 J. Phys.: Condens. Matter 21 175404

(http://iopscience.iop.org/0953-8984/21/17/175404)

J. Phys.: Condens. Matter **21** (2009) 175404 (17pp) doi:10.1088/0953-8984/21/17/175404

NMR investigations of Li^+ ion dynamics in the NASICON ionic conductors $Li_{1-x}La_{x/3}\square_{2x/3}Zr_2(PO_4)_3$

Maud Barré[1,2], Joël Emery[2,3], Pierre Florian[4], Françoise Le Berre[1,2], Marie-Pierre Crosnier-Lopez[1,2] and Jean-Louis Fourquet[1,2]

[1] Laboratoire des Oxydes et Fluorures (UMR 6010 CNRS), Université du Maine, Avenue O Messiaen, F-72085 Le Mans Cedex 9, France
[2] Institut de Recherche en Ingénierie Moléculaire et Matériaux Fonctionnels (FR 2575 CNRS), Université du Maine, Avenue O Messiaen, F-72085 Le Mans Cedex 9, France
[3] Laboratoire de Physique de l'Etat Condensé (UMR 6087 CNRS), Université du Maine, Avenue O Messiaen, F-72085 Le Mans Cedex 9, France
[4] Centre de Recherche sur les Matériaux à Hautes Températures CNRS, F-45071 Orléans Cedex 2, France

Received 8 July 2008, in final form 12 December 2008
Published 30 March 2009
Online at stacks.iop.org/JPhysCM/21/175404

Abstract

NMR studies of ^{7}Li and ^{31}P nuclei are reported in the 150–900 K temperature range for the $Li_{1-x}La_{x/3}\square_{2x/3}Zr_2(PO_4)_3$ NASICON compounds with $x = 0.8$, 0.7, 0.6 and 0.3. Magic angle spinning (MAS mode) experiments were performed at room temperature on the ^{7}Li and ^{31}P nuclei. The linewidth and the spin lattice relaxation times of these nuclei are studied versus temperature in the static mode. The spectra recorded in the MAS mode show that the ^{7}Li ions occupy three chemical sites, the occupation of which being very sensitive to the x values but not sensitive to the coexistence of the two varieties $C\bar{1}$ and $R\bar{3}c$ observed at room temperature in compounds with $x \leqslant 0.5$. On the other hand, the ^{31}P nucleus MAS spectra are very sensitive to lithium content but also to the variety coexistence. T_1 measurements were performed in a static mode on the ^{7}Li and ^{31}P nuclei. In all the compounds, the ^{7}Li spin lattice relaxation time exhibits two branches with several minima, indicating the complex dynamics for this ion. One of these minima appears in the same temperature range as the minimum of the ^{31}P nucleus T_1, strongly suggesting a cross-relaxation process between these nuclei. $T_{1\rho}$ measurements on ^{7}Li (static mode) allow us to show a slow motion different from the one probed by the T_1. The analysis of the $T_{1\rho}$ behaviour with temperature and composition allows us to ascribe the motion probed by this time to the oxygen ion motion which monitors the opening and closing of the lithium pathways. A qualitative interpretation of the ^{7}Li T_1 results is done; it takes into account the cross-relaxation phenomena between ^{31}P and ^{7}Li and quadrupolar fluctuations.

(Some figures in this article are in colour only in the electronic version)

1. Introduction

The interest in sodium and lithium ion conductors is due to their uses in electrochemical devices. Among them, the NASICON compounds, with general formula $A_xM_2(XO_4)_3$ [1] have been extensively studied [2–4]. Their structure consists of a three-dimensional network built from MO_6 octahedra and XO_4 tetrahedra interconnected by oxygen atoms [2]. Recently, we published a complete structural study of the continuous solid solution $Li_{1-x}La_{x/3}\square_{2x/3}Zr_2(PO_4)_3$ ($0 \leqslant x \leqslant 1$) [5]. This solid solution results from the substitution mechanism $Li^+ \rightarrow 1/3La^{3+} + 2/3\square$, where $\square$ stands for vacancy. Among these compounds, the $x = 0$ member $La_{1/3}\square_{2/3}Zr_2(PO_4)_3$, which crystallizes in a new space group for a NASICON

compound ($P\bar{3}$) [6], has already been completely characterized by thermal x-ray diffraction, ^{31}P NMR spectroscopy and ionic conductivity measurements [7].

Several methods are available for investigating the physical properties of the materials. Among them nuclear magnetic resonance (NMR) presents the advantages of being sensitive to the molecular motion and to providing information on the local arrangement in ordered or disordered material. Dynamical properties are obtained through the relaxation times measurements. The motion induces random fluctuations of the nuclear spin interaction which stimulate the relaxation of the spin system. However, relaxation theory needs a knowledge of the spectral densities of the motion. This step is a difficult one because we have to know the relaxation pathways that have to be modelled. So, good knowledge of the experimental data and a precise analyse of them have to precede the theory.

The aim of this paper is then to highlight the dynamical properties of the Li^+ ions in the $Li_{1-x}La_{x/3}\square_{2x/3}Zr_2(PO_4)_3$ solid solution by using the ^{7}Li and ^{31}P NMR technique in the temperature range between 150 and 1000 K: the materials under investigation are some of the $Li_{1-x}La_{x/3}\square_{2x/3}Zr_2(PO_4)_3$ members with $x = 0.8$, 0.7, 0.6 and 0.3 respectively, called hereafter Li0.2, Li0.3, Li0.4 and Li0.7. These experiments take advantage of the presence of the ^{7}Li nucleus, which is the mobile ion, and of the ^{31}P nucleus, which, embedded in its oxygen tetrahedron, participates in the material skeleton and will give information about the Li^+ ionic environment. The ^{17}O could be an interesting nucleus because in the structure the oxygen ions connect the PO_4 tetrahedra and the ZrO_6 octahedra but, owing to its low natural abundance, this nucleus was not studied. Moreover, the high ^{139}La and ^{138}La quadrupolar momentum values prevent any dynamical study of these nuclei.

To this aim, this paper includes the presentation and discussion of experimental data, coming from either magic angle spinning (MAS) experiments or obtained with the static mode used in the relaxation times T_1, $T_{1\rho}$ and linewidth (T_2) studies. After a presentation of the general experimental conditions used, the NMR results are given. The first part of this paper concerns both the structural properties and the dynamical ones (relaxation times) and are presented by dwelling on their general features. The second part of this paper will be devoted to a qualitative discussion of the nuclear magnetic relaxation mechanism.

2. Experimental procedure

2.1. Synthesis

$Li_{1-x}La_{x/3}\square_{2x/3}Zr_2(PO_4)_3$ ($0 \leqslant x \leqslant 1$) were synthesized in powder form by the complex polymerizable method as described in previous papers [5–8], using $^7Li_2CO_3$, dried La_2O_3, $ZrOCl_2{\cdot}8H_2O$ and $NH_4H_2PO_4$ in stoichiometric ratios. The use of ^{7}Li-enriched carbonate is justified by the high sensitivity of this nucleus in NMR.

2.2. NMR conditions

The MAS experiments were performed at RT on an Avance DSX300 spectrometer (Bruker) using a standard 4 mm probe and the samples were spun at 10 kHz.

The dynamical properties were studied over a large temperature range 150–1000 K in a static mode using two spectrometers: a Bruker Avance DSX300 for temperatures between 150 and 410 K and a Bruker ADX 300 for temperatures in the range RT–1000 K. The temperature overlap (RT–410 K) between the two experimental set-ups allows us to control the measurement's goodness. The two spectrometers work at Larmor frequencies $\nu_0 = 121.495$ MHz for the ^{31}P nucleus and $\nu_0 = 116.642$ MHz for the ^{7}Li one.

For temperatures between 150 and 410 K, we used a $t_{90} = 4\ \mu$s for the two nuclei. In the case of the ^{7}Li quadrupolar nucleus, this value corresponds to a non-selective excitation in the materials under consideration. The sample, glued on an altuglass holder, is placed into a 5 mm coil. Between 150 K and room temperature (RT) the sample is cooled by a regulated nitrogen flow and between RT and 410 K it is heated with a regulated airflow ($\pm$0.1 K).

For temperatures between RT up to 1000 K, the amplitude of the radio-frequency field for ^{7}Li is $\nu_1 = 15.5$ kHz. It is imposed by the high temperature NMR probe and corresponds to $t_{90} = 16\ \mu$s. This value can lead to a selective regime for our materials, depending on the amplitude of the quadrupolar C_Q parameter. The sample is placed in a high purity boron nitride crucible (Grade AX05, carborundum). The airtight fit is obtained with a screw cap. The crucible levitates in an airflow. The sample is heated with a CO_2 CW laser ($\lambda = 10.6\ \mu$m). A computer monitors its power (15–120 W). The temperature calibration is performed *in situ*, outside of the magnetic field, with a set-up having the same geometry as the experimental one. The phase transition temperature of the Na_3AlF_6 sample is used to calibrate the temperature. The temperature is controlled at about $\pm$30 K. In the two sets of experimental set-ups, the NMR probe head is flowed with an air current at room temperature.

Longitudinal relaxation times T_1 are measured on ^{7}Li in the temperature range 150–900 K by using a saturation pulse sequence. To improve the ratio signal/noise, either 64 or 128 transients were accumulated for ^{7}Li. The ^{7}Li nucleus $T_{1\rho}$ experiments are performed on resonance in the RT–420 K temperature range with the locked radio-frequency field fixed at 62.5 kHz. The ^{31}P spin lattice relaxation time was studied in the RT–420 K temperature range.

^{7}Li is a quadrupolar nucleus ($I = 3/2$) with a small quadrupolar moment ($Q = -0.045 \times 10^{-28}$ m^2). In the presence of some electric field gradient such a nucleus exhibits different transitions: central transition (CT) between $+1/2$ and $-1/2$ levels and external transitions ($\pm 1/2 \leftrightarrow \pm 3/2$). ^{31}P is a spin $I = 1/2$ nucleus.

In order to show some non-exponential behaviour in the magnetization recovery after the saturation comb, the experimental results of the ^{31}P and ^{7}Li nuclei are processed in the logarithmic scale at each temperature. In this scale the experimental function

$$\mathrm{Log}[(M_0 - M_{\exp}(\tau))/M_0] \qquad (1)$$

makes easy the evidence and the determination of the different T_1. Theses values are checked in the linear scale results. This method was particularly helpful in the study of ^{7}Li relaxation:

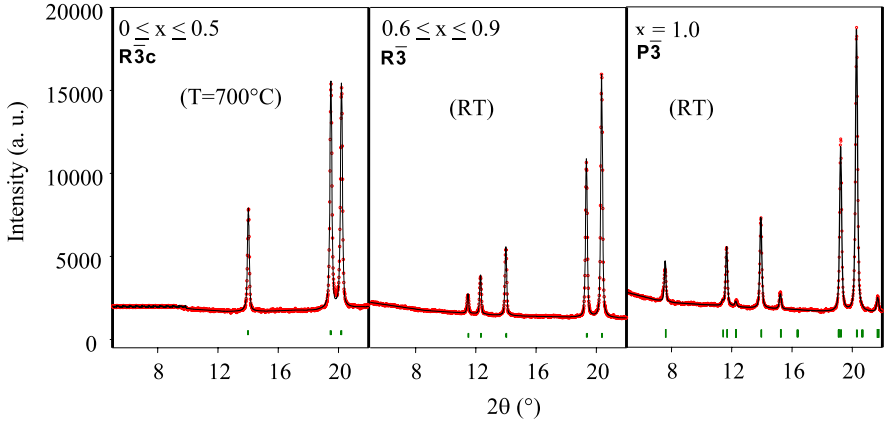

Figure 1. Typical x-ray diffraction patterns obtained for $Li_{1-x}La_{x/3}Zr_2(PO_4)_3$, depending on the x value.

owing to the $I = 3/2$ eigenvalue of the ^{7}Li nucleus angular momentum, two T_1, two T_2 and two $T_{1\rho}$ are expected with specific ratios in the slow regime (at low temperature) [9–13] if the relaxation is due to quadrupolar fluctuation. Three T_1 can be observed if there is a residual quadrupolar interaction [12]. This number has to be multiplied by the number of different sites.

The DMFIT software is used to fit the spectra and gives the linewidths, the peak positions (in Hz or ppm), the percentages and quadrupolar splitting [14]. ^{31}P spectra are referenced from H_3PO_4 (85%) and ^{7}Li from LiCl. Results are expressed either in Hz or in ppm (X(Hz) = X(ppm) × ν_0(MHz)).

3. Results

3.1. Structural description

Structural investigation of the solid solution $Li_{1-x}La_{x/3}\square_{2x/3}Zr_2(PO_4)_3$ ($0 \leqslant x \leqslant 1$) has been described in previous papers [5–7]. These studies, carried out on powder x-ray and neutron diffraction data, showed three crystallographic domains related to the NASICON family: $0 \leqslant x \leqslant 0.5$, $0.6 \leqslant x \leqslant 0.9$ and $x = 1$.

For $0 \leqslant x \leqslant 0.5$, all the compounds adopt at high temperature the typical NASICON structure (S.G., $R\bar{3}c\alpha$ variety) [15] while at lower temperature, their structure distorts to a triclinic form (S.G. $C\bar{1}$, α' variety) as observed for $LiZr_2(PO_4)_3$ prepared above 1100 °C [16]. The reversible phase transition $C\bar{1} \leftrightarrow R\bar{3}c$ is clearly soft: the two varieties α and α' coexist on a large temperature domain depending on the Li content. Table 1 gives these thermal domains of coexistence for the two forms α and α' and indicates that all the samples are biphased at room temperature for the compositions $0 \leqslant x \leqslant 0.5$.

For $0.6 \leqslant x \leqslant 0.9$, only one variety is observed whatever the temperature (S.G. $R\bar{3}$).

The member $x = 1$, $La_{1/3}\square_{2/3}Zr_2(PO_4)_3$, presents at room temperature a trigonal cell (S.G. $P\bar{3}$) [6]. At 1000 °C, a structural transition $P\bar{3} \rightarrow P\bar{3}c1$ is observed due to La^{3+} ion motion in the network $[Zr_2(PO_4)_3]^-$ [7].

It is important to note that, whatever the Li content and despite the use of neutron diffraction, we did not succeed in localizing the Li^+ ions in the structure. Nevertheless, refinements carried out at 700 °C with Li^+ ions in positions proposed by Catti *et al* [15] for $LiZr_2(PO_4)_3$ (α variety) lead to better reliability factors for the high lithium content members ($0 \leqslant x \leqslant 0.5$). This result seems to indicate that Li^+ ions occupy effectively this site whatever the members of the solid solution for such compositions. For $0.6 \leqslant x \leqslant 0.9$, due to the poor lithium content, the choice of the Catti positions does not ameliorate the reliability factors.

Table 1. Thermal domains of coexistence of the two varieties, triclinic and rhombohedral, for $0.1 \leqslant x \leqslant 0.5$.

	T (°C)							
x	100	200	300	400	500	600	700	800
0.1	$C\bar{1} + R\bar{3}c$			$R\bar{3}c$				
0.2	$C\bar{1} + R\bar{3}c$				$R\bar{3}c$			
0.3	$C\bar{1} + R\bar{3}c$					$R\bar{3}c$		
0.4	$C\bar{1} + R\bar{3}c$						$R\bar{3}c$	
0.5	$C\bar{1} + R\bar{3}c$							$R\bar{3}c$

Parts of the typical x-ray diffraction patterns obtained for samples belonging to these three crystallographic domains ($Li_{0.7}La_{0.1}\square_{0.2}Zr_2(PO_4)_3$, $Li_{0.2}La_{0.8/3}\square_{1.6/3}Zr_2(PO_4)_3$ and $La_{1/3}\square_{2/3}Zr_2(PO_4)_3$) are given in figure 1: the main difference between these three typical diffractograms is observed at low angles. Projections presented in figure 2 illustrate the different La^{3+} distributions described in $R\bar{3}c$, $R\bar{3}$ and $P\bar{3}$ space groups.

Finally, this study has shown that the substitution mechanism $Li^+ \rightarrow 1/3La^{3+} + 2/3\square$ between $LiZr_2(PO_4)_3$ and $La_{1/3}\square_{2/3}Zr_2(PO_4)_3$ induced a progressive lowering of symmetry ($R\bar{3}c \rightarrow R\bar{3} \rightarrow P\bar{3}$), as shown in table 1, due to the ordering of La^{3+} ions and vacancies in the $[Zr_2(PO_4)_3]^-$ NASICON network: in the $R\bar{3}c$ space group, the La^{3+} cations and vacancies are located on the same site (6b); in the $R\bar{3}$ space group, the La^{3+} and vacancies are located, respectively, on the 3b and 3a sites, while in the $P\bar{3}$ space group, four different sites (1a, 1b, 2d and 2d′) are available for La^{3+} and vacancies (figure 2).

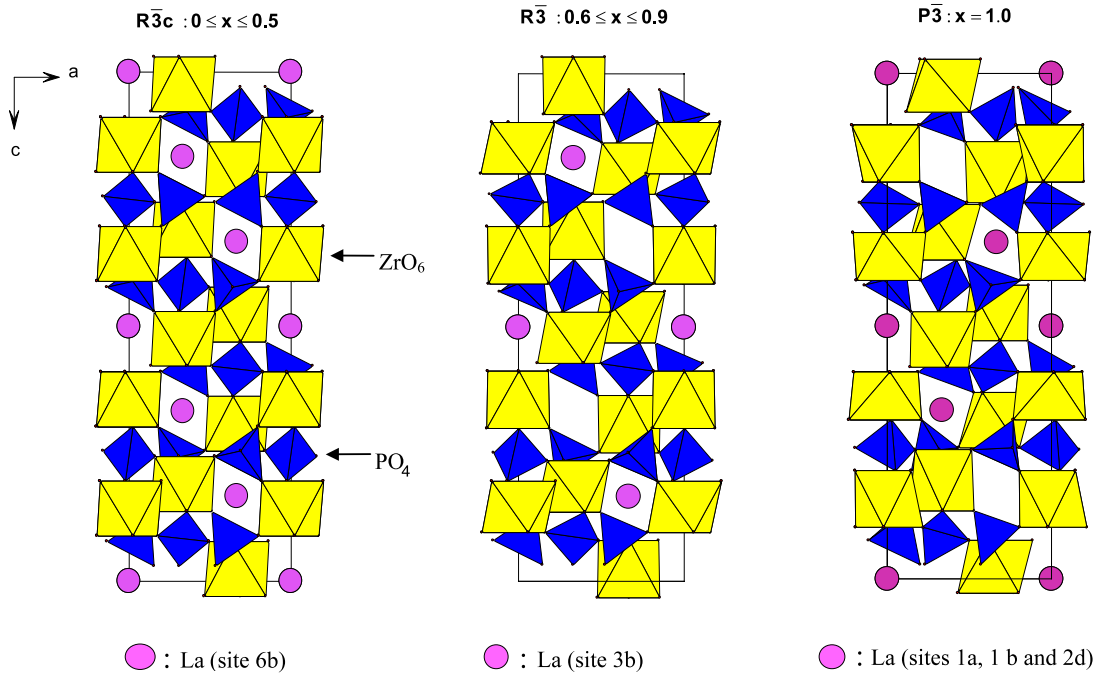

Figure 2. Evolution of $Li_{1-x}La_{x/3}Zr_2(PO_4)_3$ structure with substitution $Li^+ \rightarrow 1/3La^{3+} + 2/3\square$ ($R\bar{3}c$ for $0 \leqslant x \leqslant 0.5$; $R\bar{3}$ for $0.6 \leqslant x \leqslant 0.9$; $P\bar{3}$ for $x = 1$). Only half of the La sites are occupied in the $R\bar{3}$ structure.

3.2. NMR investigation

3.2.1. ^{7}Li high resolution. All the NMR interactions are expressed as the products of a spin operator $S^{(2)}_{\Lambda_i,m}$ and a spatial one $A^{(2)}_{\Lambda_i,m}$ which take into account the ^{7}Li neighbouring features at the i site, and the Hamiltonian is [17]

$$H_i = \sum_{\Lambda_i} C_{(\Lambda_i)} \sum_{m=-2}^{2} (-1)^m A^{(2)}_{(\Lambda_i)-m} S^{(2)}_{(\Lambda_i)m} \qquad (2)$$

where Λ_i stands for the interaction and $X^{(2)}_m$ $X^{(2)}_{(\Lambda_i)m}$ ($X = A$ or S) is the m^{th} component of the second-order irreducible tensor $\bar{\bar{X}}$. ^{7}Li is a quadrupolar nucleus with spin $I = 3/2$ subjected to chemical shift, dipolar and quadrupolar interactions. This last interaction, characterized by the parameter

$$\frac{C_{(Q_i)}}{2} = \frac{e^2 q_i\, Q}{2I\,(2I-1)\hbar} = \omega_{Q_i} \qquad (3)$$

gives a specific spectrum shape with central and satellite transitions due to the quadrupolar anisotropy $eq_i \bar{\bar{V}}(\theta_i, \phi_i)$ which accounts for the local electric field gradient at the ^{7}Li site (the angles θ_i and ϕ_i identify the direction of the static magnetic field $\vec{B}_0$ in the principal axis system of the electric field gradient tensor). The electric field gradient is defined with its amplitude eq_i and its asymmetry parameter η_{Qi}.

The ^{7}Li spectra obtained at RT in the MAS mode with a synchronized acquisition are given in figure 3 for the different members studied. Due to this specific acquisition the satellite transitions are not observed. Nevertheless, in the non-synchronized acquisition the satellite transitions are very weak or unobserved at RT. There are two main reasons. The first one concerns the quadrupolar parameter C_Q which is very weak either because the Li^+ ion is mobile and the quadrupolar interaction is averaged, or the electric field gradient is very weak at the Li^+ site (high symmetry). In the second case the quadrupolar parameter C_Q is distributed and this disorder broadens the satellite transitions at the first order of the perturbation. So when this distribution is large, the satellite transitions enter in the spectrum baseline (see below and figure 5). The central transition is broadened at the second order and it is generally the lone observable transition. In the case of the $x = 0$ member ($LiZr_2(PO_4)_3$) the satellite transitions were clearly observed [18, 19] in the static mode and this could suggest that the motion easily averages the quadrupolar splitting in the non-pure Li phases ($x \neq 0$). The area under the curve accounting for the lithium magnetization amplitude, the normalized spectra in figure 3, are in agreement with the lithium amounts in the different samples. Furthermore the linewidths increase with the lithium amount. This evolution can be attributed to an increase of the residual dipolar (homo- and/or heteronuclear) interaction or of some disorder not averaged by the MAS experiment. Any disorder also leads to a chemical shift and dipolar distributions.

The MAS spectra, as reported in figure 3(b), are analysed with three contributions called Li1, Li2 and Li3, the parameters of which are given in table 2. We observe that the different parameters are sensitive to the composition of the samples. On the well-established basis [20, 21], the line position with the most negative shift can be attributed to the longest Li–O bond as well as to the site with the highest coordination. As the crystallographic studies of the $Li_{1-x}La_{x/3}\square_{2x/3}Zr_2(PO_4)_3$ did not allow us to determine the Li positions in the NASICON structure, it is difficult to attribute the different spectral contributions to any sites in the structure. But we can expect

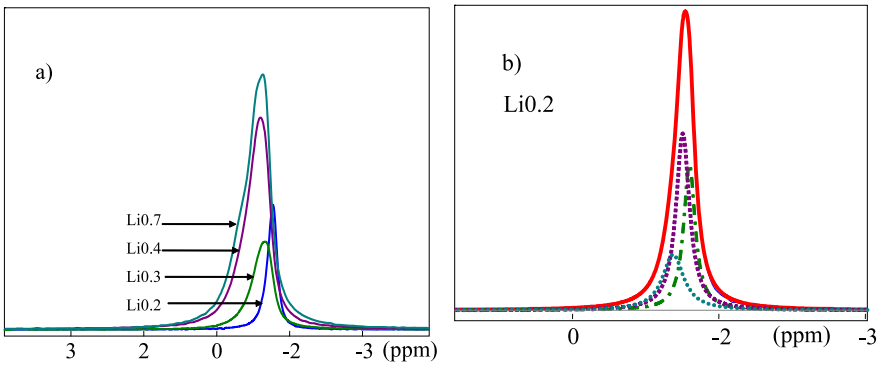

Figure 3. (a) Room temperature MAS spectra (spinning frequency 10 kHz): isotropic line for the different samples studied. (b) Fit example showing the three contributions in the Li0.2 sample.

Table 2. ^{7}Li spectral parameters for the different samples.

	δ_{iso} (ppm) $\pm$ 0.3				Linewidth (ppm) $\pm$0.1				% $\pm$2				Li content (per cell)			
	Li0.2	Li0.3	Li0.4	Li0.7	Li0.2	Li0.3	Li0.4	Li0.7	Li0.2	Li0.3	Li0.4	Li0.7	Li0.2	Li0.3	Li0.4	Li0.7
Li1	−1.4	−1.2	−1.1	−0.9	0.2	0.3	0.3	0.3	31	32	32	24	0.37	0.58	0.77	1.01
Li2	−1.3	−1.0	−0.7	−0.6	0.2	0.4	0.7	0.7	46	41	38	30	0.55	0.74	0.91	1.26
Li3	−1.2	−0.8	−1.0	−1.0	0.3	0.6	0.4	0.4	23	27	30	46	0.28	0.48	0.72	1.93

the Catti positions to be the most probable, at least for the Li0.7 member; in the average position the lithium has the same coordination. So the line in the spectra will depend only on the Li–O bond length. In each sample under investigation we can attribute three different chemical environments, called Li1, Li2 and Li3. It is worth noting that no additive contribution to the Li spectrum is observed in $Li_{0.7}La_{0.1}O_{0.2}Zr_2(PO_4)_3$ in spite of the presence of the two structural varieties ($\alpha R\bar{3}c + \alpha' C\bar{1}$). We can also remark that the linewidth in the Li2 site increases with the Li amount while it remains constant in Li1 and oscillates around 0.4 ppm in Li3.

The percentage of each contribution to the spectra can be correlated to the Li amount in each environment (last column in table 2). The three lithium site (Li1, Li2, Li3) amounts are increasing when x is decreasing. In the low lithium composition the most occupied site is Li2 while Li1 and Li3 are similarly occupied. Nevertheless, for the high lithium composition the site Li3 becomes largely the most occupied one.

Since the first (oxygen) and second (phosphorus) neighbours lead to only one chemical site for the lithium, we need, to understand the origin of the three chemically different lithium sites, to consider the third neighbours which are also the second ^{31}P neighbours: La1, La2, vacancy, Li $^{+}$. These third neighbours act on the Li–O distance and modify its chemical properties. This means also that these second neighbours could participate (at least indirectly) in the ^{7}Li relaxation mechanisms.

3.2.2. ^{31}P spectrum. The interest of the phosphorus embedded in its oxygen tetrahedron lies in its sensitivity of the second neighbour as was shown in our previous paper [6, 7]. In the present case its second neighbour can be La^{3+}, Li^{+} or vacancy. In figure 4 we reported the high resolution (MAS experiment) NMR ^{31}P spectra. The contributions marked with some stars in Li0.3 and Li0.4 (around −5 and −40 ppm) are attributed to some impurities (less than 5%). Apart these impurity contributions, the spectra spread between −20 and −30 ppm and change with the lithium amount. These spectra are reconstructed with four (in Li0.2, Li0.3 and Li0.4) or seven lines (in Li0.7), the parameters of which are given in table 3. The same four lines present in all the spectra are broad while the three further ones in Li0.7 (−23.3, −23.8 and −24.1 ppm) are narrower. The three additive contributions observed in Li0.7 account for the two structural varieties ($\alpha R\bar{3}c + \alpha' C\bar{1}$) present in this sample, but also indicate that in Li0.7 there is phosphorus with more ordered lithium and less disordered ones.

In a first step, we consider $Li_{1-x}La_{x/3}\square_{2x/3}Zr_2(PO_4)_3$ with $x \geqslant 0.5$. In comparison with the $x = 1$ member [6, 7], there is one line more. In these samples, the structural studies have shown that the phosphorus ions were located in only one crystallographic site while four chemical ^{31}P sites were observed. This difference is due to the nature of the phosphorus second neighbours: vacancy, Li^{+} or La^{3+} ions. We can reasonably think that the screening of the ^{31}P nucleus decreases from vacancy to the La^{3+} ions. So line (4) in the high field position (−29 ppm) can be attributed to the ^{31}P with vacancies as second neighbours. The two lines (1) and (2) in the lowest field region (−20 and −23 ppm) have to be attributed to phosphorus with La^{3+} as second neighbours as was established in the phase $La_{1/3}\square_{2/3}Zr_2(PO_4)_3$. The line (3) around −26 ppm has to be attributed to the ^{31}P with the Li^{+} ion as second neighbour. This conclusion is corroborated by the following remarks. When the lithium amount decreases,

- firstly, the line (4) contribution increases, indicating that the amount of vacancies increases;

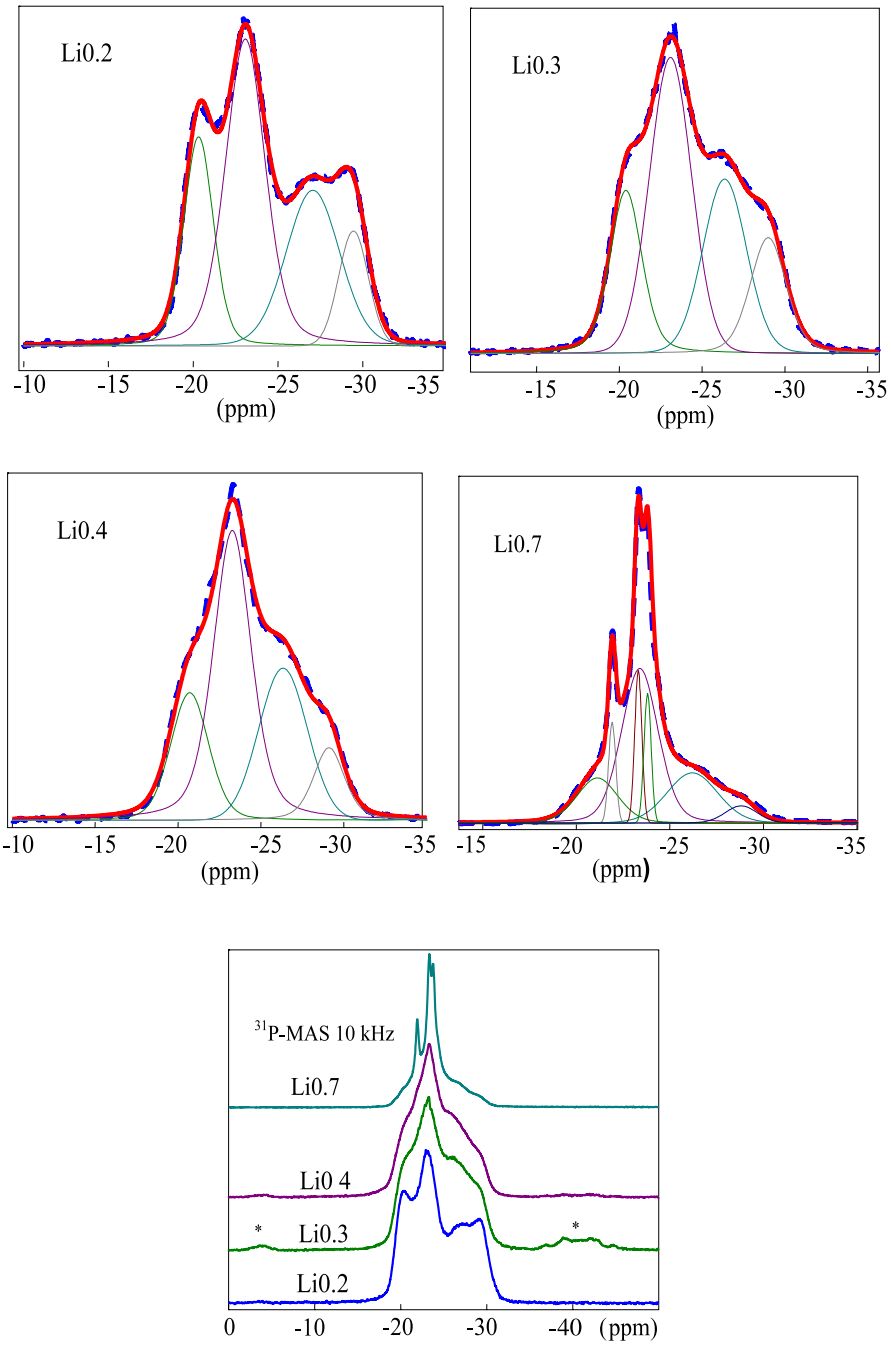

Figure 4. ^{31}P MAS experimental and calculated spectra for the different samples. In front the same spectra with a larger spectral width. In Li0.3 some further contributions marked with a star are attributed to impurities. The same remark can be made for Li0.4 with smaller extra contributions. Their contributions are less than 5%. Owing to the narrow lines in Li0.7 the spectra are not normalized.

- secondly, the sum of the contributions (1) and (2) increases, which can be attributed to an Li^+ substitution by La^{3+};
- thirdly, at the same time the contribution of line (3) decreases.

In a second step, we consider the Li0.7 sample. As mentioned above, two phases coexist in this sample, explaining why there are three more narrow lines in its spectrum. The broad lines (2, 4, 6, 7) correspond to the lines in the $x \leqslant 0.5$ samples described above. The positions of the narrow lines (1, 3, 5) correspond to the ones reported for the triclinic phase by Arbi *et al* [19] in the pure phase $LiZr_2(PO_4)_3$. The further lines are narrower because the lithium experiences a weaker disorder than in the other samples with weak lithium amount.

3.3. Dynamical aspect

3.3.1. ^{7}Li dynamics. The relaxation times (T_1, T_2 or $T_{1\rho}$) of the Zeeman energy bring information about the dynamical properties of the nucleus under consideration. The linewidth

Table 3. ^{31}P spectral parameters for the different samples.

	$Li_{0.2}La_{0.8/3}Zr_2(PO_4)_3$			$Li_{0.3}La_{0.7/3}Zr_2(PO_4)_3$			$Li_{0.4}La_{0.6/3}Zr_2(PO_4)_3$		
Lines	δ_{iso} (ppm) ± 0.2	Linewidth (ppm) ± 0.1	% ± 1	δ_{iso} (ppm) ± 0.2	Linewidth (ppm) ± 0.1	% ± 1	δ_{iso} (ppm) ± 0.2	Linewidth (ppm) ± 0.1	% ± 1
1	−20.3	2.0	21	−20.4	2.3	17	−21	3.2	25
2	−23.1	2.9	43	−23.1	3.1	45	−23.3	2.23	29
3	−26.9	3.1	20	−26.4	3.3	24	−26.1	4.1	41
4	−29.3	2.2	16	−29.3	2.5	14	−29.3	2.3	5

	$Li_{0.7}La_{0.1}Zr_2(PO_4)_3$		
Lines	δ_{iso} (ppm) ± 0.2	Linewidth (ppm) ± 0.1	% ± 1
1	−21.9	0.4	4.2
2	−22.8	4.2	45.1
3	−23.3	0.4	6.9
4	−23.7	1.4	20.2
5	−23.8	0.3	3.6
6	−26.7	3.4	16.9
7	−29.2	1.8	3.1

(related to T_2) and lineshape are also interesting parameters for this purpose.

Figure 5(a) gives the spectra for Li0.2 recorded at two temperatures in the static mode. In order to account for the experimental spectra recorded in this mode we only need a single line with a Gaussian/Lorentzian shape in the temperature range 190 K $\leqslant T \leqslant$ 600 K. The three-line structure observed in the MAS mode disappears because the dipolar broadening and the chemical shift anisotropy are not averaged. No satellite transition is observed with $t_{90} = 4\ \mu$s. This figure evidences the temperature effect on the linewidth. Figure 5(b) gives the high temperature behaviour of the ^{7}Li spectra recorded with $t_{90} = 16\ \mu$s. The two NMR probes give the same spectrum between RT and 420 K. Nevertheless, as shown in figure 5(b), the presence of a static disorder is also expected. In this figure the arrow indicates the temperature (above 600 K, depending on the sample) at which the dipolar broadening and/or the disorder is sufficiently averaged to allow the emergence of a broad component. At the lowest temperature at which it was clearly distinguished from the baseline, the ratio between the narrow and the broad component is nearly the theoretical 4:6 ratio between the central and satellite transitions. This means that the motion partially averages the distribution of the quadrupolar interaction. We can note that, in the presence of a very broad component, the excitation can be a selective one, especially in the case of the high temperature experiment for which the excitation time is $t_{90} = 16\ \mu$s. Nevertheless, when these satellite transitions are observed we are in the non-selective excitation regime. This fact will not change our results about the relaxation times apart from the ratio between the two relaxation times for the quadrupolar ^{7}Li nucleus with $I = 3/2$ spin and the cross-relaxation mechanism. As the satellite transitions are not observed at RT we can think they are due to specific motion which makes these transitions observable: the average position of the ion vibration is shifted, giving rise to an electric field gradient component which is not averaged by the motion. Then with the increase of the amplitude of the anisotropic electric field gradient fluctuations the satellites are partially averaged, leading to a better resolution of the satellite transitions.

The Gaussian/Lorentzian shape used to account for the ^{7}Li spectrum recorded in the static mode is given by x_gG + (1 − x_g)L, where x_g stands for the Gaussian (G) contribution and (1 − x_g) for the Lorentzian (L) one. G and L have the same position and the same linewidth. The x_g factor entering in the lineshape evolves with temperature, as is represented in figure 6. At low temperature, the Gaussian contribution is the same for all the samples. Between 200 and 250 K, this contribution decreases all the more since the sample is rich in lithium. Up to 450 K, this contribution increases. Above this temperature, the Gaussian contribution decreases to zero and the line becomes Lorentzian, showing the ionic motion effect. Apart from the deepening of the minimum which depends on the lithium amount (the deeper the minimum is the higher the lithium amount is), the x_g behaviour is the same for all the samples: three domains are observed: rigid lattice at low temperature (RL), intermediate (I) in which the interactions are partially averaged and the high temperature domain (HT) in which the interactions are averaged. In figure 6, the arrows in the intermediate regime indicate a temperature at which some change in the linewidth behaviour is also observed in figure 7.

This x_g parameter behaviour with temperature is rarely observed after decreasing when the temperature continues to increase; it is very surprising because we expect the lineshape to remain Lorentzian at high temperature. This behaviour is certainly due to the presence of the three lithium sites as observed in the MAS mode with different dipolar broadenings and chemical shift anisotropy. Nevertheless, this behaviour is not due to the satellite transitions which appear at higher temperature.

The experimental linewidths versus reciprocal temperature for the different samples are given in figure 7. The linewidth is also a good indicator of the motion. Out of the rigid lattice rapid regime, it is given by $\ell \propto \ell_0 \tau_c$, where ℓ_0 is the linewidth in the rigid lattice and τ_c is the correlation time

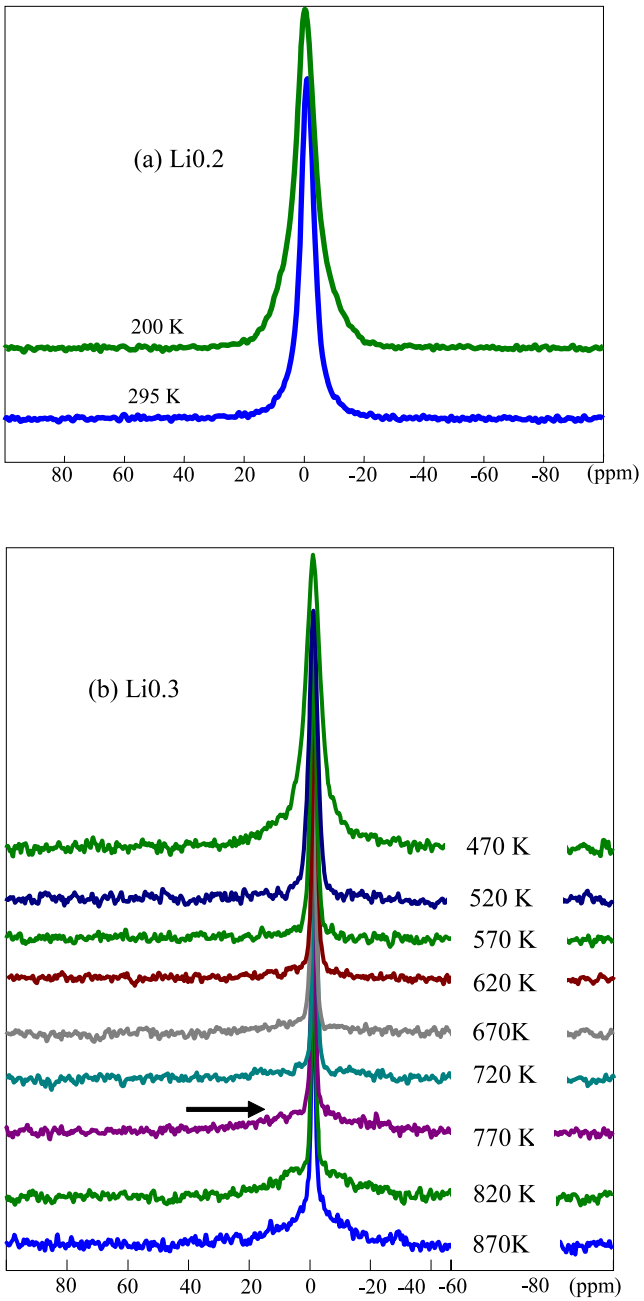

Figure 5. (a) ^{7}Li spectra for the Li0.2 sample recorded in the static mode at different temperatures. This figure shows the narrowing effect due to the activated motion (first NMR probe with $t_{90} = 4\ \mu$s). (b) ^{7}Li spectra versus temperature recorded with the second NMR probe ($t_{90} = 16\ \mu$s). A broad component attributed to the satellite transition begins to merge at 770 K (arrow). The ratio limit at high temperature between the two contributions is 4:6, corresponding to the ratio between the central and the satellite transitions.

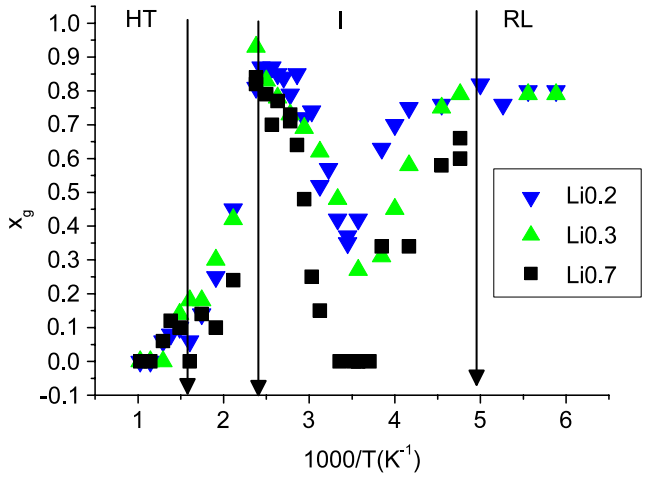

Figure 6. Gaussian contribution to the lineshape versus the temperature. Below the RL arrow (210 K) the system is in the rigid lattice regime and above the HT arrow the system is in the complete motional narrowing regime. This behaviour is common to all the samples. The arrow in the intermediate regime indicates the temperature at which some change in the linewidth also appears.

of the motion. At low temperature (rigid lattice limit), the line broadens when the lithium amount increases. This can perhaps be due to some disorder in the lithium sites but mainly to some changes in the dipolar interactions and in the chemical shift anisotropy. This was also observed in MAS spectra at room temperature. Above 220 K ($1000/T = 4.5$), the linewidth decreases owing to the correlation time decrease: the motion averages, at least partially, the dipolar interaction but also averages the disorder. At 445 K ($1000/T = 3.25$) a second regime in the decrease appears at the same temperature as the one at which the x_g parameter decreases again. At $1000/T = 2.25$ a third linewidth behaviour change is observed corresponding to the decrease of the x_g parameter. The dipolar interaction contribution to the lithium linewidth in the rigid lattice limit can be a good indicator in order to obtain information on the Li positions. This contribution is given by the Van Vleck relation [22]:

$$(M_2)^2 = f_Q \frac{3}{5}\gamma_I^4\hbar^2 I(I+1)\left(\frac{\mu_0}{4\pi}\right)^2 \sum_j \frac{p_i p_j}{r_{Ij}^6} + \frac{4}{15}\gamma_I^2\gamma_S^2\hbar^2 S(S+1)\left(\frac{\mu_0}{4\pi}\right)^2 \sum_m \frac{1}{r_{Im}^6}. \quad (4)$$

This relation gives the dipolar contribution to the second moment in a powdered sample, p_i being the probability for the lithium to be at the i site. The first term accounts for the like spins (lithium) coupling and the second one to the unlike spins (phosphorus ions essentially, because, owing to their low γ factor, we do not take the zirconium ions into account). The spin I is the observed one, γ_I and γ_s parameters are the gyromagnetic ratios and r_{Im} is the distance between the I and m spins. The f_Q parameter differentiates the resonant I-like spins: $I{:}f_Q = 1$ if $I = 1/2$, $f_Q = 9/10$ in the case of spin 3/2 with the same quadrupolar interaction or $f_Q = 4/5$ with different quadrupolar interaction [17, 23], p_j is the probability for a spin of the same I kind to be at the site j. As explained in the structural part, it was not possible to find Li^+ ion positions and then to calculate the rigid lattice second moment. Nevertheless this second moment can be evaluated by taking the lithium at an average position which can be taken as the lanthanum one. The second moment calculated values due to the dipolar interaction are 1.2, 0.9, 0.8 and 0.6 in ppm for Li0.7, Li0.4, Li0.3 and Li0.2, respectively. The main contribution is due to the heteronuclear

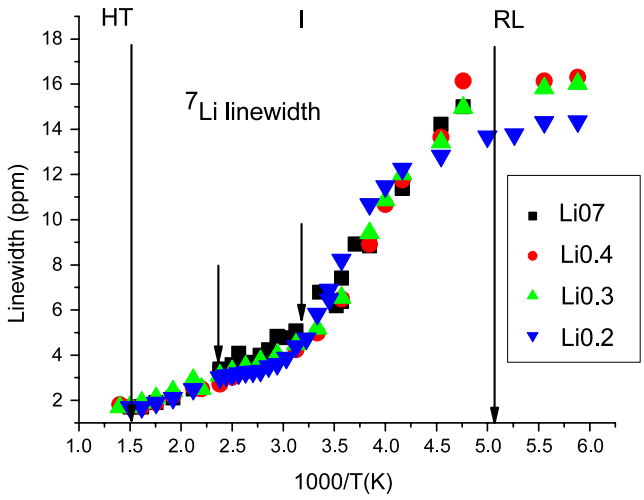

Figure 7. ^{7}Li spectrum linewidth in the static mode versus the reciprocal temperature are reported for the different samples. The three regions defined in figure 6 are also represented. In this temperature range the spectra consist of the central transition and are not sensitive to any satellite transition effects. The arrows in the intermediate regime indicate a change in the linewidth behaviour (see also figure 6).

contribution (Li–P) given by the second term in (4). These values are weaker than the experimental linewidth (between 14 and 16 ppm in the rigid lattice limit). There are two main reasons for these differences. The first one concerns the position of the lithium; in our calculation we supposed it was an average position determined from the lanthanum one. This calculation shows that this hypothesis is wrong. The other reason could be another contribution to the linewidth due to some chemical shift anisotropy because any disorder in the quadrupolar interaction acts at second order on the central transition. Furthermore, the linewidth at high temperature (rapid regime), which is in the range of the ones obtained in the MAS spectra, prove that the broadening is not due to quadrupolar parameter distribution but due to an interaction which can be averaged both by the coherent rotation in the MAS experiment and the fluctuation. So the linewidth of the central transition is an indicator for the fluctuation amplitudes which average the interaction. So we can understand that in the first step the satellite transitions are not averaged.

3.3.2. ^{7}Li spin lattice relaxation T_1. In the case of an activated motion, one of the general features of the T_1 curve versus temperature is the presence of one minimum. The relaxation rate $R_1 = 1/T_1$ is the inverse of the corresponding relaxation time and measures the probability per second that the spin system exchanges Zeeman energy under the influence of the fluctuations. The position of the T_1 minimum is defined by $\omega_0\tau_c \approx 1$ which separates the slow regime $\omega_0\tau_c \gg 1$ in the low temperature range and the rapid regime $\omega_0\tau_c \ll 1$ in the high temperature one. $\omega_0 = 2\pi\nu_0$ where ν_0 is the ^{7}Li Larmor frequency. τ_c is the correlation time of the motion at temperature T. In figure 8, we report the experimental spin lattice relaxation rates R_1 versus the reciprocal temperature. Figure 8(b) shows that two branches called R_1^f (fast T_1) and R_1^s (slow T_1) are observed in all the samples. Figure 8(a) gives a global insight into the T_1 behaviour. Only the R_1^f component is represented in order to keep some visibility. Figure 8 shows the presence of several maxima on each branch and for each sample. It is worth noting that our experimental results and the ones obtained in the pure lithium phase $LiZr_2(PO_4)_3$ [18] are similar. In this last case the experiments were performed at 16.5 MHz.

The ratio of the two relaxation times does not correspond to the one expected when the relaxation is due to the pure quadrupolar fluctuation. Moreover, the contributions change with temperature. At room temperature these ratios cannot be ascribed to any lithium kind Li1, Li2 or Li3 (see table 2). Finally the two relaxation times seem to transform into a single one in the rapid regime (above $1000/T \cong 1$); this is particularly well shown in the case of the Li0.2 and Li0.3 samples. These remarks lead us to ascribe these two relaxation times to a specific feature of the dynamical process which is neither due to any pure ^{7}Li quadrupolar spin character nor to the presence of several Li^+ sites as observed in the MAS spectra. Nevertheless the mixing of different relaxation mechanisms has to be considered as is suggested by the x_g parameter behaviour.

The most surprising fact is the presence of several maxima (called A, B, C, D, E and F) in the fast R_1^f relaxation curves while four maxima are observed in the R_1^s one. This multiplicity of maxima is not due to any phase transitions. Let us consider the R_1^s curves in the different samples. The B, D, E and F maxima are the most obviously shown ones in the Li0.3 sample. In Li0.2 the B and D maxima are also well in evidence; the E and F ones are very close but can also be distinguished. The D, E and F maxima are also well observed in the R_1^s curve in Li0.7. Nevertheless, in Li0.4 there are some difficulties in seeing the two relaxation rates D and E. The D maximum on the R_1^s curve is the most obviously observed in all the compounds where it appears at the same temperature. Finally five maxima called A, B, C, D and E are also observed on the R_1^f curves in the same temperature ranges where the maxima are observed on the R_1^s curve. On the R_1^f curve, the D maximum remains at the same temperature (770 K) in the different compounds. The E maximum position oscillates between 200 and 290 K. Its position is at 220 K in Li0.2 and at 270 K in the other compounds. Apart from the A, B and D maxima, it is not so easy to define their positions on the R_1^f curve but they nearly appear in the same temperature ranges as the one on the R_1^s curve. The D maximum is the most sensitive to the composition.

So, with the obtained results on the two relaxation rate curves R_1^f and R_1^s, we can come to the conclusion that there are six maxima, more or less observable, in the different samples. These maxima appear when the fluctuation correlation time τ_c is in the range of the inverse of the Larmor frequency: $\omega_0\tau_c \approx 1$. In these experiments the measured correlation time is the same ($\tau_c = 1.4 \times 10^{-12}$ s) for the six peaks but this value is reached at different temperatures corresponding to different τ_{co} values and/or different activation energies E_a in the case of an activated motion with $\tau_c = \tau_{c0}e^{\frac{E_a}{kT}}$. It is worth noting that the E peak shift toward the high temperature corresponds to an

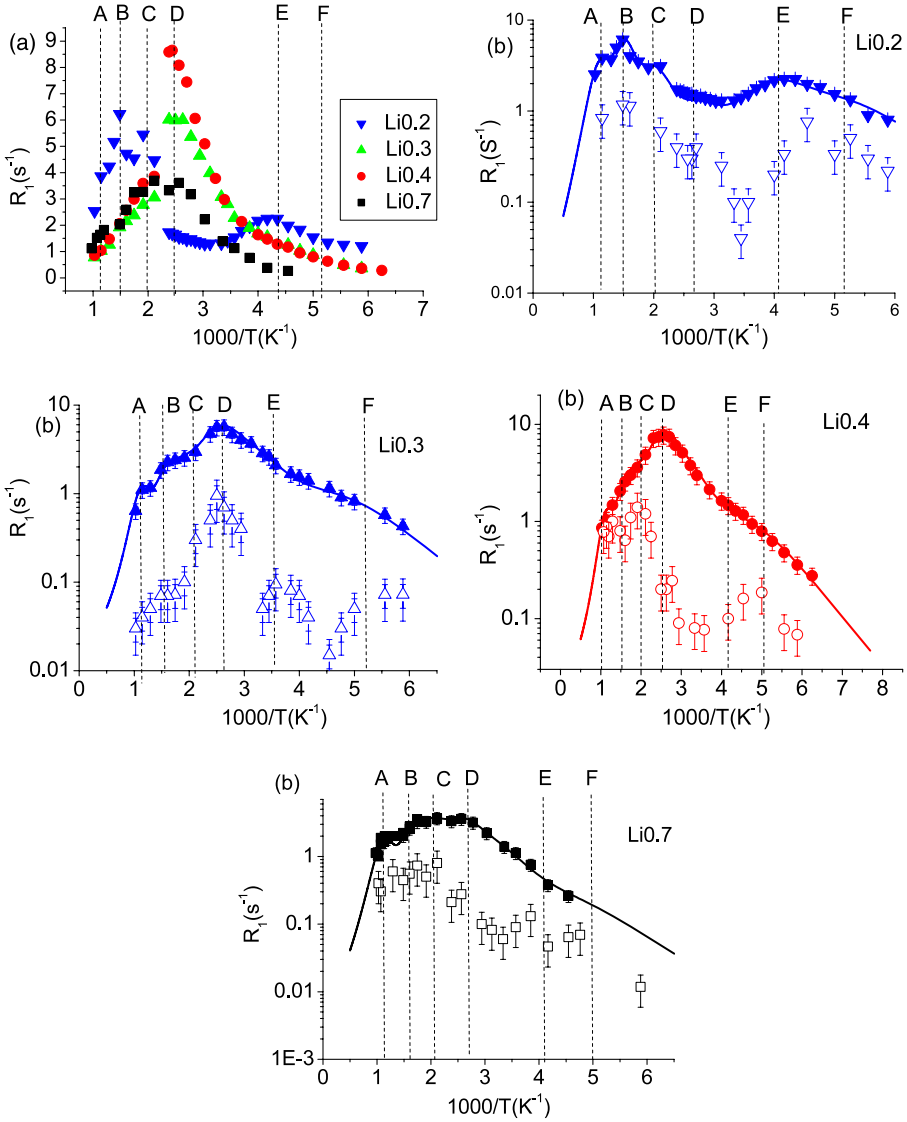

Figure 8. Experimental spin lattice relaxation rates $R_1 = 1/T_1$ versus the reciprocal temperature for the different samples. The vertical lines named A, B, C, D, E and F indicate approximately the positions of the maximum either on the fast T_1 or the slow one. (a) Rapid rates in the linear scale allow us to evidence different maxima. (b) Two times account for the relaxation of the magnetization: a fast one (full symbol) and a slow one (open symbol). The experimental error on the fast T_1 is around 10% when it is around 30% on the slow one. The line on the rapid rate is a guide for the eye.

increase of the τ_{c0} parameter and to a decrease of the attempt jump frequency.

The D peak of the spin lattice relaxation rate exhibits a maximum for Li0.4 ($x = 0.6$) as can be observed in figure 8. The same behaviour is observed for the mobility which is reported in table 4. It is worth noting that in Li0.4 the activation energy measured by conductivity σ_{dc} is comparable to the one observed in $LiZr_2(PO_4)_3$ [18]. Following the fluctuation–dissipation theorem [24], the mobility at the angular frequency ω is given by the relation

$$\mu(\omega) = \beta \int_0^\infty \mathrm{d}t\, \mathrm{e}^{\mathrm{i}\omega t} \langle \vec{u}(t)\vec{u}(0)\rangle$$

which is the Fourier transform of the ion velocity correlation function $\vec{u}(t)$, with $\beta = \frac{1}{kT}$ and k is the Boltzmann constant. The velocity correlation function is related to the one of the position, and we know that the fluctuation amplitudes of the spatial Hamiltonian parameters are related to the fluctuation positions.

Table 4. Conductivity results in the different samples. Li0.4 shows a net mobility maximum.

Composition	E_a (eV)	σ_{dc} at 400 K (10^{-4} S cm^{-1})	Mobility at 400 K (10^{-11} m^2 V^{-1} s^{-1})
Li0.2	0.49 (3)	0.34 (1)	2.7 (1)
Li0.3	0.41 (3)	1.58 (1)	8.7 (1)
Li0.4	0.38 (4)	3.55 (1)	14.0 (1)
Li0.7	0.40 (3)	0.34 (1)	8.8 (1)

An interesting observation has to be made between the x_g parameter and the T_1 curve: for all the compositions, these two parameters both exhibit a behaviour change at $1000/T = 3.5$

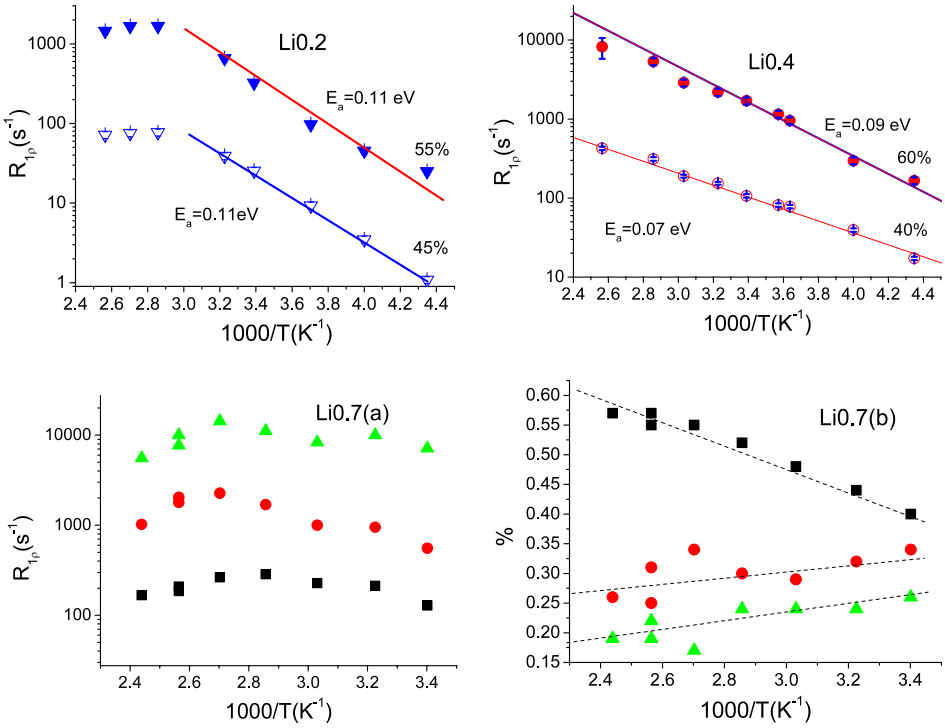

Figure 9. Spin lattice relaxation rate in the rotating frame versus reciprocal temperature in Li0.2, Li0.4 and Li0.7(a). The different contributions are independent of the temperature in Li0.2 and Li0.4 while they are dependent in Li0.7.

and 2.5. This is an indication of a change in the dynamical mechanism.

3.3.3. ^{7}Li spin lattice relaxation time in the rotating frame $T_{1\rho}$. The ^{7}Li spin lattice relaxation in the rotating frame $T_{1\rho}$ and the associated relaxation rate $R_{1\rho} = 1/T_{1\rho}$ allow us to probe slow motions (long distance motion or motion of a large mass as the polaron one) with characteristic frequency $\nu_1 = \omega_1/2\pi$ ($\omega_1 = \gamma B_1$). In our experiments, $\nu_1 = 62.5$ kHz. The experimental results concerning Li0.2, Li0.4 and Li0.7 are reported in figure 9. It can be observed that, at each temperature in the studied range allowed by our device, two $T_{1\rho}$ are observed in Li0.2 and Li0.4, when three $T_{1\rho}$ are observed in Li0.7.

The contributions are independent of the temperature in Li0.2 and Li0.4 while they change in Li0.7. In Li0.4 these contributions are 0.6 for the fast $T_{1\rho}$ and 0.4 for the slow $T_{1\rho}$, while in Li0.2 the two contributions are respectively 0.55 and 0.45. These ratios do not correspond to the one expected for the $I = 3/2$ spin when a pure quadrupolar relaxation is alone implied; moreover, in this case only one $T_{1\rho}$ remains in the fast regime (at high temperature after the maximum). In Li0.2 and Li0.4, at room temperature, these contributions correspond to the ones of the lithium contents (see table 2): (Li1 + Li3) for the fast $R^{\mathrm{f}}_{1\rho}$ rate and Li2 for the slow one $R^{\mathrm{s}}_{1\rho}$. In Li0.2 the two contributions have nearly the same activation energy $E_{\mathrm{a}} = 0.1$ eV, in Li0.4 the activation energies are weaker and slightly different. In Li0.7, at room temperature, the contributions correspond to the one obtained from the spectra. Furthermore the three $T_{1\rho}$ appear weakly activated and seem to go through their maxima. So the $T_{1\rho}$ differentiates the lithium sites observed in the spectrum while the T_1 does not. Such a $T_{1\rho}$ property was already reported in the literature [25] in other compounds.

In order to understand the behaviour of the $T_{1\rho}$ contributions in Li0.7 it is worth recalling the presence of two varieties $R\bar{3}c$ and $C\bar{1}$ in this composition. When temperature is increasing the phase $C\bar{1}$ disappears. Unfortunately, our device does not allow to reach sufficiently high temperatures in order to observe this disappearance. Nevertheless, it seems that the $T_{1\rho}$ results account for this change when the spectrum does not.

In Li0.2, the $R_{1\rho}$ maxima are clearly reached at $1000/T \approx 2.7$ for the two curves while in Li0.4 we only observe a clear tendency toward a maximum for the fast $T_{1\rho}$. In Li0.7, the three contributions reach their maxima at $1000/T \approx 2.8$. The fluctuation correlation time can be obtained at $1000/T$ around 2.7 ($T \approx 370$ K) in Li0.2 with the relation $\omega_1\tau_{\mathrm{c}\rho} = 2\pi\nu_1\tau_{\mathrm{c}\rho} \approx 1$, which gives $\tau_{\mathrm{c}\rho} = 2.5\times10^{-6}$ s. This value cannot be compared with the value $\tau_{\mathrm{c}} = 10^{-12}$ s obtained from the maxima of the spin lattice relaxation rate R_1. In Li0.4 the maximum will be reached at higher temperature; this means the correlation time $\tau_{\mathrm{c}0\rho}$ is higher in this sample than in Li0.2.

Although in this temperature range ($2.4 < 1000/T < 3.4$) peak D in the T_1 curve begins to grow, there is no correlation with the change in the $T_{1\rho}$ curve because such a motion with $\tau_{\mathrm{c}0\rho} = 9.2\times10^{-8}$ s and $E_{\mathrm{a}} = 0.1$ eV cannot show any minimum $\omega_0\tau_{\mathrm{c}} \cong 1$ of relaxation at positive temperature. So, $T_{1\rho}$ probes a very different motion than the ones observed by T_1. Nevertheless it is worth noticing that in this temperature range both the linewidth and the x_{g} parameter behaviour

change. In this temperature range no effect is observed in the phosphorus T_1 curve (see below).

The two spin lattice relaxation rates in the rotating frame are more important (one decade) in Li0.4 than in Li0.2. The range of the three $T_{1\rho}$ values in Li0.7 covers the one both in Li0.2 and Li0.4. As the correlation times and the activation energies are very similar in the three compounds the difference arises from the amplitude of fluctuations. This result agrees with our previous conclusion about the relation between the spin Hamiltonian parameter fluctuation amplitudes and the mobility of the ion.

The use of the relation $R_{1\rho}(^7\text{Li}) \approx \frac{[\Omega_{1\rho}(^7\text{Li})]^2}{\omega_1(^7\text{Li})}$ allows us to evaluate the fluctuation amplitude $[\Omega_{1\rho}(^7\text{Li})]$ at the maximum of the $R_{1\rho}$ curves. In Li0.2 we obtain

$$\Omega_{1\rho}(^7\text{Li}) = 28 \times 10^3 \text{ rad s}^{-1} \text{ for (Li1 + Li3) contributions}$$

$$\Omega_{1\rho}(^7\text{Li}) = 6.3 \times 10^3 \text{ rad s}^{-1} \text{ for Li2 contribution.}$$

By applying the same relation at the maxima of the three $R_{1\rho}$ curves of the Li0.7 sample we obtain

$$\Omega_{1\rho}(^7\text{Li}) = 35 \times 10^3 \text{ rad s}^{-1} \text{ for Li1 contribution}$$

$$\Omega_{1\rho}(^7\text{Li}) = 11.2 \times 10^3 \text{ rad s}^{-1} \text{ for Li2 contribution}$$

$$\Omega_{1\rho}(^7\text{Li}) = 3.5 \times 10^3 \text{ rad s}^{-1} \text{ for Li3 contribution.}$$

These results give information about the fluctuation amplitudes at the different Li1, Li2 and Li3 sites.

The activation energy obtained from T_1 relaxation times data by using a single exponential correlation function is generally much lower than the activation energy obtained by dc-conductivity experiments. This result, generally encountered in conductors, can be ascribed to one or several of the following reasons: (i) NMR is sensitive to dimensionality in contrast to dc conductivity, (ii) different time scales between the two experiments are probed: NMR measurements are performed at 116 MHz while a σ_{dc} regime is found below 1 MHz at 300 K and (iii) different length scales are probed: T_1 obtained by NMR probes ionic local motion while σ_{dc} probes the charge carrier long range one. Nevertheless, $T_{1\rho}$ probes motion in the range probed by σ_{dc}. So we expect the activation energy to be the same for $T_{1\rho}$ and σ_{dc}. The activation energy values obtained from both T_1 and $T_{1\rho}$ do not correspond to the one obtained by σ_{dc}. Nevertheless, we found that the highest $R_{1\rho}$ also corresponds to the highest mobility as T_1.

As a first insight we can say that the lithium ion jumps between two cages with the frequency $1/\tau_{c\rho}$, and it jumps between different sites inside each cage with the frequency measured by T_1. The jumps between cages give rise to two fluctuation amplitudes (28 and 6 kHz in Li0.2) depending on the neighbourhood of the nucleus. So, the long correlation time measured by $T_{1\rho}$ gives an insight into the weak activated libration motion of the phosphate tetrahedron. This motion modifies the oxygen positions. These ions build up the pathways through which the lithium ions go from one cage to the neighbouring one. So the parameter $\tau_{c0\rho} \approx 9.8 \times 10^{-8}$ s could be understood as being the average time for the opening or the closing of these pathways.

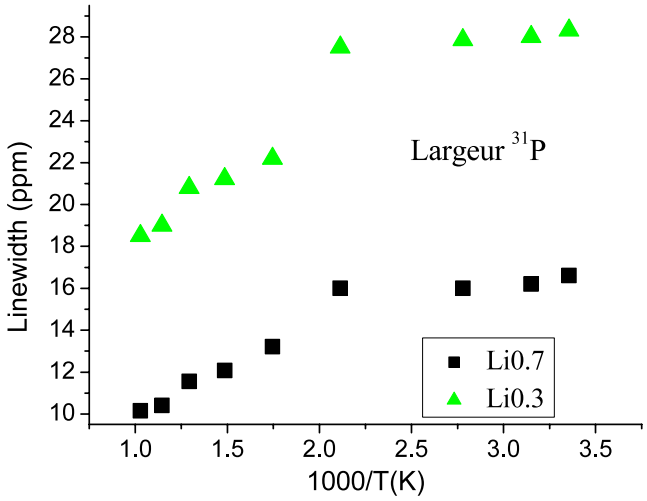

Figure 10. ^{31}P linewidth versus reciprocal temperature.

The presence of several $T_{1\rho}$ indicates that the motion is also sensitive to the second neighbours of the phosphorus ions. Such a situation corresponds to some polaron effects in which the Li particle moves in correlation with its neighbourhood. This is a strong argument for anisotropic fluctuations. Then, if we attribute the $T_{1\rho}$ to the polaron effects corresponding to the motion of the Li ion with its neighbour, we can summarize the $T_{1\rho}$ behaviour as follows: in the phase rich in lithium (Li0.7), in which there is a phase superposition, each of the three lithium ions Li1, Li2 or Li3 experiences its own low frequency motion with its own amplitude of fluctuation. Then, in the Li0.4 sample, in which only one phase is observed, the most rapid contribution of Li0.7 and the slower one remain; the first one corresponds to Li2 and the second one to (Li1 + Li3) contributions. For the lower lithium amount, only the two weakest relaxation rates observed in Li0.7 remain corresponding to (Li1 + Li3) on the one hand and Li2 on the other.

3.3.4. ^{31}P dynamics. In order to clarify the complex ^{7}Li motion shown by the ^{7}Li spin lattice relaxation time, we performed the study of the ^{31}P behaviour with temperature on a static sample. Owing to its long T_1, only two samples, Li0.3 and Li0.7, were studied at high temperature. The phosphorus nucleus possesses an $I = 1/2$ spin value and then is only sensitive to dipolar and chemical shift fluctuations.

The linewidth of the ^{31}P phosphorus measured in a static mode is sketched in figure 10. The homonuclear contribution has to remain nearly constant as arising from the structural backbone which remains rigid, so the temperature variation is essentially due to the {^{7}Li–^{31}P} heteronuclear contribution. We can also note that the line is narrower in Li0.7 than in Li0.3. This is surprising because we expect the dipolar interaction to have more effect when the lithium amount increases and broadens the line as it was observed in the lithium spectra where the lines are broader in Li0.7 than in Li0.3. On the one hand, this cannot be due to the narrow lines observed in

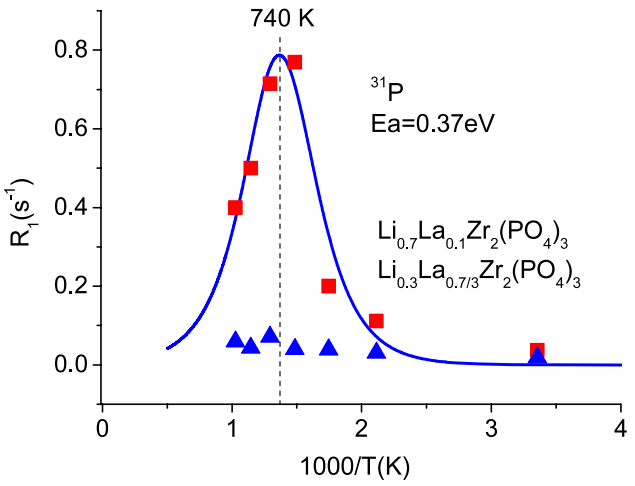

Figure 11. ^{31}P spin lattice relaxation rate versus reciprocal temperature. The activation energy is obtained from the high temperature side point. The line is a guide for the eye.

MAS experiments because they have small contributions. On the other hand, this can be due to the chemical shift anisotropy. Furthermore the dipolar contributions to the second moment of the phosphorus spectrum are weaker than the linewidth; they are 1.65, 1.7, 1.8 and 2.2 ppm for Li0.2, Li0.3, Li0.4 and Li0.7, respectively. So the linewidth is sensitive to the chemical shift anisotropy.

The experimental results of the phosphorus relaxation rates $R_1(^{31}\mathrm{P})$ are sketched in figure 11 for the limiting samples Li0.3 and Li0.7. Despite of the presence of several sites as observed in the MAS spectra, only one T_1 is observed. It remains nearly constant from room temperature to 500 K. This certainly is due to the oxygen screening, the tetrahedron of which remains relatively rigid during its libration motion and prevents any interaction fluctuations. Above 500 K, the slope of this curve becomes more important but, nevertheless it remains weak in the two samples. We can think that the Li^+ motion disturbs the oxygen positions and in return act on the dipolar coupling between the lithium and the phosphorus. It is worth noting that the decrease of the ^{31}P linewidth begins when its spin lattice relaxation rate R_1 begins to increase. The phosphorus nuclei in Li0.7 clearly evidences a shorter relaxation time and a weaker linewidth than in Li0.3. This figure also shows the importance of the lithium amount in the ^{31}P relaxation process. Keeping in mind that the T_1 in the pure lanthanum phase is around 120 s at room temperature, these results show that the ^{7}Li–^{31}P heteronuclear dipolar interaction has to be an important contribution to the phosphorus relaxation and will also influence the ^{7}Li relaxation.

Figure 11 shows that the ^{31}P relaxation is activated. The activation energy $E_a = 0.37$ eV can be extracted from these data, leading to the correlation time values at the maximum ($T = 710$ K): $\tau_c = 1.3 \times 10^{-9}$ s if we use $\omega_0\tau_c \approx 1$ or $\tau_c = 3 \times 10^{-8}$ s if we use $[\omega_0(^7\mathrm{Li}) - \omega_0(^{31}\mathrm{P})]\tau_c \approx 1$ as given by relation (9) (see below). For an activated motion with the energy $E_a = 0.37$ eV these values give $\tau_{c0} = 3.9 \times 10^{-12}$ s in the first case and $\tau_{c0} = 1.1 \times 10^{-9}$ s in the second case.

The observed T_1 values are relatively short compared to the one generally observed for this nucleus embedded in its oxygen tetrahedron. In each sample studied, the relaxation rate seems to exhibit a maximum at nearly the same temperature at which the ^{7}Li relaxation rate also exhibits some maximum. Furthermore, the $T_1(^{31}\mathrm{P})$ value is in the range of the long $T_1(^7\mathrm{Li})$ and the $T_1(^{31}\mathrm{P})$ value decreases when the lithium amount increases. The fluctuation amplitude $\Omega(^{31}\mathrm{P})$ can be deduced from the R_1 experimental maximum: $R_1(^{31}\mathrm{P}) \approx \frac{\Omega(^{31}\mathrm{P})^2}{\omega_0(^{31}\mathrm{P})}$. Figure 11 gives with $R_1(^{31}\mathrm{P}) \cong 0.8$ leading to the value $\Omega(^{31}\mathrm{P(Li0.7)}) \cong 10^4$ rad s^{-1}. The relation $R_1(^{31}\mathrm{P}) \approx \frac{\Omega(^{31}\mathrm{P})^2}{|\omega_0(^7\mathrm{Li}) - \omega_0(^{31}\mathrm{P})|}$ gives $\Omega(^{31}\mathrm{P(Li0.7)}) \cong 2 \times 10^3$ rad s^{-1}.

Taking the maximum on the Li0.3 experimental $R_1(^{31}\mathrm{P})$ curve around 0.08 (as given by T_1 in the pure phase) we can obtain $\Omega(^{31}\mathrm{P(Li0.3)}) \cong 3 \times 10^3$ rad s^{-1}. The square of the Li content ratio given in table 2 for these two compounds is 5.4; this value is in the range of the ratio between the Ω values determined above. We can also observe that these ratios are preserved even if we take the pulsation difference $|\omega_0(^7\mathrm{Li}) - \omega_0(^{31}\mathrm{P})|$ as it appears in the first term of (9) and (10).

4. Discussion

4.1. Substitution effects of the Li^+ by La^{3+}

In the pure Li phase $LiZr_2(PO_4)_3$ only one line is observed in the ^{7}Li NMR spectrum [18, 19]. In the high temperature form ($R\bar{3}c$), the ^{7}Li signal displays an axial symmetry ($\eta_Q = 0$) when in the triclinic $C\bar{1}$ form (low temperature); the signal is also reproduced with one quadrupolar line with ($\eta \neq 0$). In the rhombohedral form, the static ^{7}Li NMR spectrum displays a narrowing effect associated with an increase of the mobility. In this phase Petit and Sapoval [18] conclude from crystallographic data and linewidth behaviour that the theoretical lithium site splits into six equivalent positions to conserve the D_{3d} symmetry. As a consequence of the Li motion between these six sites an averaged axial symmetry is observed. In the compounds where the Li^+ ion is substituted by the La^{3+} cation, the crystallographic data are better analysed with the lithium ions in the Catti positions (36f) [15]. These positions, which correspond to M3 type sites, are intermediate between M1 and M2 sites and can only be occupied by small cations. This Li localization in the 36f site seems to be confirmed by our second moment calculation. There are six equivalent Catti positions (D_{3d} local symmetry) which are found on two equilateral triangles shifted along the three axes. In the studied systems the ^{7}Li NMR spectra are analysed with three contributions without quadrupolar structure. So the main effect of the substitution is to differentiate the lithium environment, i.e. to differentiate the Catti positions which become non-equivalent. During its local motion (as detected by T_1) the lithium jumps between them. Some disorder in these positions and/or a quadrupolar interaction in the order of the inverse of the relaxation time ($\omega_Q\tau_c \cong 1$) could explain the non-observation of the satellite transition up to 770 K, as reported in figure 5.

The ^{31}P spectra account both for the substitution and the lithium amount in the samples. Moreover, it also accounts for the coexistence of the two varieties α and α' which is also shown by x-ray diffraction.

4.2. Behaviour of the ^{7}Li lineshape

We can summarize the important observations concerning the dynamical properties. Firstly, the three temperature domains observed in the x_g parameters versus temperature are also observed in the linewidth curves and in the T_1 curves versus temperature. Secondly, the contributions of the two relaxation times observed in ^{7}Li do not correspond either to the ones expected for the pure $I = 3/2$ quadrupolar spin relaxation or for the different contributions observed at room temperature in the high resolution spectra. Thirdly, six maxima in the spin lattice relaxation rate versus temperature are observed. Five of them (R_1^s curve) A, B, C, D and F seem to not shift and remain at their positions in the different samples while the E peak position oscillates in the range $3.5 \leqslant 1000/T \leqslant 4.5$ when the lithium amount changes.

The x_g parameter behaviour (figure 6) versus the temperature together with the linewidth one exhibit a particular behaviour. This cannot be ascribed to an exchange process because in this case some line broadening should appear in the intermediate regime while our results show a continuous decrease. The minimum depth depends on the lithium amount: the higher the lithium amount is the deeper is the minimum. This difference can be ascribed to some disorder in the lithium position which can be observed on the phosphorus MAS spectra: in Li0.7 the lines are narrower than in the other samples. Another reason could be an anisotropic ^{7}Li motion.

In order to elucidate the x_g parameter behaviour, we have to consider the lineshape with the correlation time. Under some hypothesis [17], the transverse magnetization is

$$M_y(t) = M_0\, \mathrm{e}^{-\int_0^t (t-\tau)G(\tau)\,\mathrm{d}\tau}$$

where $G(t)$ is the lattice parameter fluctuation correlation function:

$$G(t) = \sum_n \langle A_{-n}^{(2)}(t) A_n^{(2)}(0)\rangle. \tag{5}$$

In the case of a single exponential correlation function with an isotropic process we have

$$G(t) = \Delta\, \mathrm{e}^{-\frac{t}{\tau_c}} \tag{6}$$

with Δ the fluctuation amplitude and τ_c the correlation time. Such model was used by Bloembergen, Purcell and Pound [26] (BPP model). In [27] the authors consider anisotropic correlation.

The sum takes into account all the lattice parameter fluctuations found in the Hamiltonian (2). In most encountered cases all these parameters have the same correlation function and

$$G(t) = G(0)g(t) = M_2 g(t) \tag{7}$$

with $\int_0^\infty G(t)\,\mathrm{d}t = M_2\tau_c$, where M_2 is the rigid lattice second moment of the line in the case of dipolar interaction. The two limiting cases [17] correspond to

- $M_2\tau_c^2 \gg 1$: from 0 to t $G(t)$ can be considered as constant and equal to $G(0)$. The lineshape is a Gaussian one, $M_y(t) = M(0)\,\mathrm{e}^{-\frac{M_2}{2}t^2}$.
- $M_2\tau_c^2 \ll 1$: the spin system is rapidly decorrelated with $\tau_c \ll t$ and the integral limit t can be changed in infinity, giving a Lorentzian lineshape $M_y(t) = M(0)\,\mathrm{e}^{-M_2\tau_c t}$.

Between these two limit cases the lineshape is nearly the convolution of a Gaussian and a Lorentzian function; the use of the x_g parameter being a very good approximation. Nevertheless the mono-exponential behaviour of the correlation function leads to a monotonic change from Gaussian to Lorentzian lineshape when the temperature increases and the correlation time becomes weaker and weaker.

So, to account for the specific behaviour of the x_g parameter, we at least need two second moments with their own correlation times: a broad one M_B with the correlation time τ_{cB} and a narrow one M_N with its correlation time τ_{cN}. This hypothesis is supported by the behaviour of the linewidth which exhibits a change at the same temperature ($1000/T \cong 2.2$) at which x_g decreases again.

For an activated motion the correlation times evolve with temperature: $\tau_{cB} = \tau_{cB0}\mathrm{e}^{\frac{E_{aB}}{kT}}$ and $\tau_{cN} = \tau_{cN0}\mathrm{e}^{\frac{E_{aN}}{kT}}$. The broad component with the stronger activation energy E_{aB} monitors the low temperature range behaviour when the narrow E_{aN} component with the weaker activation energy monitors the intermediate temperature behaviour. Now there are four limit cases corresponding to the x_g behaviour.

- $M_B\tau_{cB}^2 \gg 1$ and $M_N\tau_{cN}^2 \gg 1$ the lineshape is Gaussian.
- $M_B\tau_{cB}^2 \ll 1$, $M_B \gg M_N$ and $M_N\tau_{cN}^2 \gg 1$ the lineshape is Lorentzian.
- $M_B\tau_{cB}^2 \ll 1$, $M_B \approx M_N$ and $M_N\tau_{cN}^2 \gg 1$ the lineshape is Gaussian.
- $M_B\tau_{cB}^2 \ll 1$ and $M_N\tau_{cN}^2 \ll 1$ the lineshape is Lorentzian.

Apart from the change from the rigid lattice to the intermediate domain I, the linewidth in figure 7 exhibits another change at $\frac{1000}{T} \approx 2.5$. At $\frac{1000}{T} \approx 3.5$, x_g again increases when temperature is increasing and the linewidth shows saturation beginning. These results agree with the mechanism presented above. From the linewidth experimental results reported in figure 7, we can deduce, $E_{aB} = 0.05$ eV, $\tau_{cB0} = 10^{-12}$ s and $E_{aN} = 0.004$ eV, $\tau_{cN0} = 10^{-12}$ s.

The broad component cannot be due to the satellite transitions because in this temperature range if these transitions exist they enter in the baseline and are not observable. So, we are only looking at the central transition in which there are several contributions to its linewidth (quadrupolar, dipolar, chemical shift). This result means that the interactions responsible for the broadening have not the same correlation function and we can expect anisotropic relaxation effects. The behaviour of the central transition width with temperature which increases before decreasing when the temperature is increasing [12] could also contribute to the specific behaviour of the x_g parameter.

These two activation energies and correlation times induce some changes in the local coupling experienced by the lithium ion. This change in temperature has several origins, three of them being

- the average positions of the ion vibrations change with the temperature and the lithium ions access to new sites;
- the lithium motions and/or the lithium neighbouring motion change with the temperature. These physical processes lead to several features.

In the first way, in agreement with the other results, we retain that in solids the motion can be anisotropic, giving rise to different correlation functions for the $A_n(t)$ lattice parameters, defined with different activation energies E_{an} and different correlation times τ_{c0n}. So, in solids a single anisotropic interaction can lead to several maxima in the relaxation rate.

In the second way, several types of interaction (chemical shift, quadrupolar, homo and hetero nuclear dipolar) with different dynamics can be implied in the relaxation of the nuclear magnetization. We can also mention the possibility of the broadening of the satellites and central transition to vary in different ways. For example, in the case of a pure quadrupolar relaxation, when the temperature is increasing, the central linewidth begins to increase, then it decreases [12]; at the same time the satellite transition linewidths is continuously increasing. Furthermore, as above, each of these interactions can also exhibit some anisotropic features.

In the third way the lithium ion accesses different sites when the temperature is increasing. This hypothesis was already mentioned with the emergence of the satellite transition. Each of these sites is characterized by its own activation energy and, inside the well, the lithium ions oscillate with the same frequency $1/\tau_{c0}$. For example, this is made possible by the oxygen motions which open other pathways when the temperature increases and the lithium accesses new sites. It is very important to note that in this case the dipolar interaction between ^{7}Li and ^{31}P is modified because the average distance $d(^7\text{Li}–^{31}\text{P})$ is modified. Then, this way could explain why the linewidth in Li0.3 is higher than in Li0.7 when we expect a dipolar ^{7}Li–^{31}P higher in Li0.7 than in Li0.3 (see figure 10). It could also explain that some quadrupolar interaction appears when temperature is increasing from a state in which it was zero (figure 5(b)).

In all the cases the interaction parameters in (2) change with temperature, leading to some different second moment contributions from the ones introduced above. Furthermore, and as underlined above, the x_g parameters and the T_1 one both exhibit some change at the same temperature. So these two changes at $1000/T = 2.5$ and 3.5 have to be due to some changes in the interactions and/or in some changes in the $A_n^{(2)}$ parameter correlation functions which originate from some changes in the Li^+ local neighbouring. So the study of the relaxation has to be divided at least into two domains: $1000/T > 3.5$ and $1000/T < 3.5$.

4.3. Qualitative interpretation of the T_1 results

A complete understanding of the relaxation process which gives rise to the multiple T_1 maxima needs a deep analysis which is beyond this paper. Nevertheless a qualitative analysis of the relaxation process can be given. Furthermore the multiplicity of the T_1 maxima observed in these samples indicates that the bulk properties, such as the ones obtained by the conductivity (which gives one activated energy value), are not related in a simple way to the single-particle motion probed by NMR.

On the one hand, when there is no residual quadrupolar interaction, it is well established for a spin $I = 3/2$ that two branches with one maximum can be observed in the T_1 curves versus temperature [9–13]. In the rapid regime only one relaxation time monitors the relaxation. The same general features are also theoretically determined for T_2 and $T_{1\rho}$. Unfortunately, in solids, it is difficult to observe the two expected relaxation times in the slow regime with the good ratio [23, 25] and only one relaxation time is often observed. This behaviour was generally attributed to spin diffusion effects which modify the nuclear level populations. Furthermore, if the heterodipolar fluctuations are also implied in the relaxation process a second maximum can be observed on the relaxation rate curve. On the other hand, when there is some quadrupolar residual interaction, three branches can be observed on the T_1 curve [12] with one maximum if the relaxation mechanism is due to pure quadrupolar fluctuation and two maxima in the other cases (pure homodipolar fluctuations, heteronuclear fluctuations and mixed fluctuations). This second maximum, due to flip-flop terms in the dipolar interaction, appears at low temperature even with a single exponential correlation function (see relation (9)). These flip-flop terms generate cross-relaxation [12, 17, 28]. So our $T_1(^7\text{Li})$ result analysis takes place in the case of a residual quadrupolar interaction with several interactions that lead to specific behaviours [12].

The ^{31}P T_1 relaxation results indicate that the relaxation process of this nucleus: (i) accelerates in the temperature range where the ^{7}Li relaxation rate also exhibits a maximum; (ii) strongly depends on the lithium amount; (iii) in the pure La phase the ^{31}P spin lattice relaxation time is 100 s and (iv) furthermore the ^{7}Li slow relaxation rate is of the same order as the ^{31}P one. These remarks indicate that the ^{31}P relaxation is strongly influenced by the lithium amount and are strong indications for a cross-relaxation mechanism in spite of the single relaxation time observed for ^{31}P.

The cross-relaxation mechanism can appear between ^{7}Li–^{31}P and ^{7}Li–^{139}La and ^{31}P–^{139}La. It is worth noting that cross-relaxation can also occur between the levels of the quadrupolar nuclei. To our knowledge, the case in which three types of nucleus are implicated in the cross-relaxation process was not studied up to now, either from a theoretical point of view or experimentally.

If we do not take into account the quadrupolar features of the lithium and lanthanum nuclei and the quantum mechanical aspect of the problem, the longitudinal magnetization relaxation for three coupled I, S and J spins which undergo a cross-relaxation process verify the Solomon macroscopic equations [28]:

$$\begin{aligned}
\frac{\mathrm{d}}{\mathrm{d}t}\langle I_z\rangle &= -R_{II}\langle I_z\rangle - R_{IS}\langle S_z\rangle - R_{IJ}\langle J_z\rangle \\
\frac{\mathrm{d}}{\mathrm{d}t}\langle S_z\rangle &= -R_{SS}\langle S_z\rangle - R_{SI}\langle I_z\rangle - R_{SJ}\langle J_z\rangle \\
\frac{\mathrm{d}}{\mathrm{d}t}\langle J_z\rangle &= -R_{JJ}\langle J_z\rangle - R_{JI}\langle I_z\rangle - R_{JS}\langle S_z\rangle
\end{aligned} \tag{8}$$

showing that the dynamics of one kind of magnetization (^{7}Li, for example) depends on the dynamics of the other magnetization kinds (^{31}P and ^{139}La). So each magnetization is monitored by three relaxation times (inside each spin system and between two types of spin systems). Nevertheless we never experimentally observe more than two branches in the T_1 results. Different reasons can cause such an observation:

(a) two of these branches are superposed;
(b) one cross-relaxation process appears at low temperature and the other one at high temperature;
(c) in some temperature range the two T_1 branches arise from cross-relaxation between the most sensitive nuclei {^{7}Li–^{31}P} and in the other temperature range the two branches arise through the quadrupolar relaxation mechanism. Furthermore the phosphorus T_1, which is strongly influenced by the lithium amount, indicates some cross-relaxation between these nuclei.

In the (b) and (c) cases the cross-relaxation appears between two spins [12, 28]. In a first approximation, the (c) case could correspond to our results because the lanthanum stands further from the ^{7}Li than the ^{31}P does, and it possesses a low gyromagnetic ratio γ.

So, in the (c) case, for a heteronuclear dipolar coupling between one spin 3/2 (^{7}Li) with one spin 1/2 (^{31}P) and in the case of a correlation function as given by (6) the T_1^{aa} and σ_{ab} parameters are [12]

$$\frac{1}{T_1^{aa}} = R_{aa} = \frac{1}{6}\frac{\mu_0^2\hbar^2\gamma_a^4}{16\pi^2} I_a(I_a+1)\Delta_{Daa}^2\tau_c \times \left\{\frac{1}{1+(\omega_a-\omega_b)^2\tau_c^2} + \frac{3}{1+\omega_a^2\tau_c^2} + \frac{6}{1+(\omega_a+\omega_b)^2\tau_c^2}\right\} \quad \text{and} \tag{9}$$

$$\frac{1}{T_{ab}} = R_{ab} = \frac{1}{18}\frac{\mu_0^2h^2\gamma_a^2\gamma_b^2}{16\pi^2}\Delta_{Dab}^2 I_a(I_a+1)\tau_c \times \left\{-\frac{1}{1+(\omega_a-\omega_b)^2\tau_c^2} + \frac{6}{1+(\omega_a+\omega_b)^2\tau_c^2}\right\} \tag{10}$$

with Δ_{Dxy} the dipolar fluctuation amplitude and the subscript a or b designates the ^{7}Li or ^{31}P nucleus.

Nevertheless, each nucleus can also be subjected to other relaxation processes (such as quadrupolar or homodipolar) which are accounted by another term in the diagonal matrix element:

$$R_{aa}^T = R_{aa} + R_{aa}^1.$$

The resolution of this differential equation system gives the two eigenvalues:

$$R_1^{\pm} = \frac{R_{aa}^T + R_{bb}^T \pm \sqrt{(R_{aa}^T - R_{bb}^T)^2 + 4R_{ab}R_{ba}}}{2}. \tag{11}$$

This shows that the magnetizations M_a or M_b are recovered with two relaxations times: a fast one associated with the rate $R_1^f = R_1^+$ and a slow one associated with the relaxation rate. In the case of an isotropic relaxation mechanism, the R_1^f curve exhibits two maxima: an absolute one and a relative one corresponding to one maximum in the R_1^s curve. It is worth noting that the first term in (9) and (10), i.e. the flip-flop terms in the relaxation mechanism, will bring the most important contribution and will enhance the spectral densities when $|(\omega_I - \omega_S)|\tau_c \approx 1$; a relative maximum observed in the high temperature side is due to the other terms.

The absolute maximum and the relative one are well separated in the ^{7}Li–^{31}P case because these nuclei resonance frequencies are very close (116 and 121 MHz) and the term with the frequency difference in (9)–(11) becomes very important. It is also possible to obtain a similar curve for the pair {^{7}Li–^{139}La} but the maxima will be less separated because their resonance frequencies (116–44 MHz) are very different.

So our results suggest the following schema in order to explain the complexity of the relaxation process. The multi-maximum features could be due to the possibility of the lithium to accede to different sites with different energies with mixed relaxation mechanisms in the case of a residual quadrupolar interaction. So, as is shown by the x_g parameter behaviour, it is possible to distinguish two domains: a low temperature one between 150 and 300 K and a high temperature one above 300 K. These two domains are clearly observed in the T_1 curves of the Li0.4 and Li0.7 samples. The F and E peaks account for the relaxation in the low temperature domain and the A, B, C and D peaks account for the high temperature one. In the low temperature domain, the relaxation is monitored by the heterodipolar interaction and the cross-relaxation gives two T_1. The low temperature domain contribution could be due to the cross-relaxation terms between ^{7}Li and ^{31}P. In the high temperature range accounted by the peaks A, B, C and D the quadrupolar interaction may monitor the relaxation with two T_1 in the slow regime and only one T_1 in the rapid regime. The failure of the theoretical contribution expected for the $S = 3/2$ quadrupolar spin may be due to the presence of several interactions in this temperature range. We can note the possible cross-relaxation between ^{7}Li and ^{139}La could also appear in the high temperature range (A, B, C).

5. Conclusion

The NMR experimental data reported in this paper concerns both the structural aspect and the Li^+ dynamics in the $Li_{1-x}La_{x/3}\square_{2x/3}Zr_2(PO_4)_3$ system in order to gain an insight into the ionic motion mechanism. We analysed the general features of the spectra and of the relaxation times T_1 and $T_{1\rho}$ of the ^{7}Li nucleus and the T_1 of ^{31}P versus temperature.

Three ^{7}Li different chemical sites are shown in the MAS spectra, the occupation of which depends on the composition. In the lower lithium concentration compounds, four ^{31}P chemically different sites are observed, one of them corresponding to the lithium as a phosphorus second neighbour, the three other sites being the ones encountered in the lanthanum pure phase $La_{1/3}\square_{2/3}Zr_2(PO_4)_3$. In the high lithium concentration compound, the superposition of the two phases α and α' is shown in the ^{31}P spectra while it is not observed in the ^{7}Li spectra.

Two ^{7}Li spin lattice relaxation times are observed at each temperature in the different compounds. The two T_1 branches

(versus temperature) show several maxima. These multi-branches and multi-maximum features were both analysed in terms of mixed fluctuations in the case of residual quadrupolar interaction with cross-relaxation mechanism.

Two $T_{1\rho}$ are observed in Li0.2 and Li0.4 when three $T_{1\rho}$ are shown in Li0.7. Their ratio is related to the spectral contributions. In Li0.2, the two $T_{1\rho}$ clearly exhibit a minimum, leading us to conclude the presence of another motion with characteristic frequency equal to 62.5 kHz around 420 K. This weakly activated motion is different from the one probed by the T_1. Furthermore the two or three $T_{1\rho}$ branches mean that there are two or three lithium sites which differ by their fluctuation amplitudes.

The rapid motion probed by the T_1 is attributed to a motion between Catti sites belonging to the same cage while $T_{1\rho}$ is attributed to a slow motion between sites belonging to different cages and takes into account their neighbourhood; it can also be attributed to polaron effects. This result is very important because it can contribute to the understanding of $T_{1\rho}$ in other compounds [23].

We have also shown that the ^{31}P nucleus relaxation is strongly influenced by the lithium amount. These curves exhibit a maximum in a temperature range in which the short T_1 of ^{7}Li also exhibits a maximum and this maximum amplitude strongly depends on the ^{7}Li amount. Furthermore, the ^{31}P T_1 value is in the range of the long ^{7}Li T_1 component one. These results were analysed as a strong indication for a cross-relaxation process between the lithium and phosphorus. An experiment with a heterodecoupling in which the ^{31}P nucleus is irradiated when the ^{7}Li one is observed could confirm this hypothesis but, unfortunately, the ^{31}P and ^{7}Li close frequencies prevent such an experiment with our NMR probe.

It is now evident that these experimental results and their preliminary analyses need a deeper theoretical investigation. To go further in the ^{7}Li nucleus T_1 spin lattice relaxation investigation, the knowledge of the correlation function for the spin Hamiltonian parameters appears to be the most crucial problem. This knowledge cannot be obtained by neutron diffraction and some modelling steps seem to be necessary. A relaxometry experiment at fixed temperature and variable frequency could differentiate between an intrinsic multi-potential well system or a single potential which changes with temperature. Such an experiment would complete the origin of the satellite transitions which merge at high temperature.

Acknowledgment

One of us (JE) would like to thank D Petit at Ecole Polytechnique-Palaiseau-France for stimulating discussion.

References

[1] Sljukic M, Matkovic B, Prodic B and Scavnicar S 1967 *Croat. Chem. Acta.* **39** 145
[2] Hagman L O and Kierkegaard P 1968 *Acta Chem. Scand.* **2** 1822
[3] Hong H Y-P 1976 *Mater. Res. Bull.* **11** 173
[4] Alamo J 1993 *Solid State Ion.* **63–65** 547
[5] Barre M, Crosnier-Lopez M P, Le Berre F, Suard E and Fourquet J L 2007 *J. Solid State Chem.* **180** 1021
[6] Barré M, Crosnier-Lopez M P, Le Berre F, Emery J, Suard E and Fourquet J L 2005 *Chem. Mater.* **17** 6605
[7] Barré M, Le Berre F, Crosnier-Lopez M P, Bohnke O, Emery J and Fourquet J L 2006 *Chem. Mater.* **18** 5486
[8] Pechini M P 1967 *US Patent Specification* 3330697
Kakihana M 1996 *J. Sol–Gel Sci. Technol.* **6** 7
[9] McLachlan A D 1964 *Proc. R. Soc.* A **280** 271
[10] Hubbard P S 1970 *J. Chem. Phys.* **53** 985
[11] Bull T E 1972 *J. Magn. Reson.* **8** 384
[12] Petit D and Korb J P 1988 *Phys. Rev.* B **37** 5761
[13] Delville A, Porion P and Faugère A M 2000 *J. Phys. Chem.* B **104** 1546
[14] Massiot D, Fayon F, Capron M, King I, Le Calvé S, Alonso B, Durand J-O, Bujoli B, Gan Z and Hoaston G 2002 *Magn. Reson. Chem.* **40** 70
[15] Catti M, Comotti A and Di Blas S 2003 *Chem. Mater.* **15** 1628
[16] Iglesias J E and Pecharroman C 1998 *Solid State Ion.* **112** 309
[17] Abragam A 1961 *Les Principes du Magnétisme Nucléaire* (Paris: Presses Universitaires de France)
[18] Petit D and Sapoval B 1986 *Solid State Ion.* **21** 293
[19] Arbi K, Ayadi-Trabelsi M and Sanz J 2002 *Chem. Mater.* **12** 2985
[20] Alam T M, Conzone S and Brow R K 1999 *J. Non-Cryst. Solids* **258** 140
[21] Xu Z and Stebbins J 1995 *Solid State NMR* **5** 103
[22] Van Vleck J H 1948 *Phys. Rev.* **74** 1168
[23] Kamb K and Ollom J F 1956 *J. Phys. Soc. Japan* **11** 50
[24] Kubo R, Toda M and Hashitsume N 1983 *Statistical Physics I and II* (*Springer Serie in Solid-State Science*) 2nd edn (Heidelberg: Springer)
[25] Emery J, Bohnké O, Fourquet J L, Buzaré J Y, Florian P and Massiot D 2002 *J. Phys.: Condens. Matter* **14** 523
[26] Bloembergen N, Purcell E M and Pound R V 1948 *Phys. Rev.* **73** 679
[27] Kristensen J H and Farnam I 2002 *J. Magn. Reson.* **158** 99
[28] Solomon I 1955 *Phys. Rev.* **99** 559